A Z-Source-Based Bidirectional DC Circuit Breaker With Fault Current Limitation and Interruption Capabilities

Davood Keshavarzi, Teymoor Ghanbari, and Ebrahim Farjah, *Member, IEEE*

***Abstract*—DC microgrids have some attractive characteristics, which have being investigated to utilize in future electrical power systems. However, they have several essential challenges, such as limiting and interrupting fault current, which should be rectified to have high-performance dc microgrids. In this paper, an efficient dc bidirectional fault current limiter and interrupter (FCLI) based on Z-source topology is proposed to overcome some of the challenges in dc microgrids. The FCLI is a multifunction device, by which power flow direction control, circuit breaking, fault current limiting, and interrupting in a dc system can be handled. Analytical analysis of the FCLI is discussed in detail for different operation modes. Performance of the proposed FCLI in the different operation modes is evaluated using some simulations and experiments. The results confirm high capability of the device to realize appropriate operation in dc systems. Fast response time of fault current limitation and interruption, simple and reliable structure, and negligible conduction loss are the main features of the proposed FCLI.**

***Index Terms*—Circuit breaker, dc microgrid, interrupter, multifunction, Z-source breaker.**

I. Introduction

In RECENT decades, some economic and environmental motivations lead to remarkable development of using distributed generation (DG) based on renewable energy sources (RES). Microgrids are suitable network structures, which have been proposed for these DGs [1]–[3]. The microgrids consist of DGs, energy storage systems, and variable sensitive and nonsensitive loads, which interact to each other in a certain contract. Microgrids can be broadly categorized into ac and dc types, which may operate in grid-connected and standalone operation modes [4]–[6]. Since most of the RES and static power storage systems, such as photovoltaic cells, fuel cells, batteries, and supercapacitors, have dc output power, dc microgrids have more economic and technical justifications for them. For such resources, in comparison with ac microgrid, dc microgrids have some advantages, such as reduction of power losses and power conversion stages, ease of implementation and control, no need of voltage or reactive power control, and connection of power sources without any synchronization [7]. However, there are some challenges with the dc microgrids, such as lack of practical experiences, guidelines, and standards. Moreover, some protection issues, such as 1) breaking dc arc, 2) diagnosis of fault types, 3) fault location, are more controversial in comparison with ac microgrid [8], [9].

Quenching arc upon tripping of protective devices is the most important concern. Arc reduces lifetime of circuit breakers and increases cost of maintenance [10]–[12]. In ac microgrids, arc between a circuit breaker contacts is extinguished naturally because there is zero crossing in current waveform. In dc networks, there is no zero crossing in current or voltage to quench arc in dc circuit breakers. In addition, dc fault current magnitude and rise time are high due to ratio of L and R. Consequently, fault current interruption and limitation are encountered with some challenges because of stress on the switches. One solution to this problem is using oversized ac breakers instead of dc breakers, which is expensive and large in scale [13]. Another solution is using hybrid circuit breaker, which conducts normal current by a mechanical switch and interrupts fault current by a parallel solid-state switch [14]. The last option is using solid-state circuit breakers, in which both the normal current conduction and fault current interruption are relegated to the solid-state switch [15].

Traditional solid-state circuit breakers have an auxiliary forced commutation circuit, by which the main switch is turned off in zero voltage switching or zero current switching without any arc [16]–[18]. However, the required auxiliary switching circuitry increases cost and complexity of the breaker. Moreover, fault detection delay time should be taken into account in the design considerations. Nevertheless, in critical fault condition, fast detection and accurate timing for the forced commutation is too complicated. Recently, *L–C* connection Z-source circuit breakers have been proposed to tackle these problems. The first Z-source circuit breaker has been proposed in [19]. This valuable reference conducts several investigations to have more efficient dc circuit breakers. The first structure of Z-source circuit breaker is also improved to handle load change condition and limitation of the capacitor current in [20]. In [21], a series design of Z-source breaker is proposed. The *L–C* configuration has been suggested for an impedance-fed inverter, which can operate in voltage and current modes in [22]. In this converter, turning on both switches of one leg, called shutting-through

Manuscript received May 5, 2016; revised June 30, 2016 and August 31, 2016; accepted October 17, 2016. Date of publication November 1, 2016; date of current version April 24, 2017. Recommended for publication by Associate Editor D. Xu.

The authors are with the School of Electrical and Computer Engineering, Shiraz University, Shiraz 71847-64175, Iran (e-mail: davood.kesha1370@gmail.com; ghanbarih@shirazu.ac.ir; farjah@shirazu.ac.ir).

Color versions of one or more of the figures in this paper are available online at http://ieeexplore.ieee.org.

Digital Object Identifier 10.1109/TPEL.2016.2624147

state, is not only a concern but helps to realize the converter functions. This capability of Z-source topology is used for fault current interruption in dc power systems.

In general, in a Z-source circuit breaker, transient fault current is passed through some capacitors by which the main SCR is forced commuted in a current zero crossing. Therefore, this natural commutation provides a fast fault clearance process. However, Z-source circuit breakers may have maloperation in case of low transient faults. For handling such faults by a Z-source circuit breaker, an auxiliary forced commutation circuit is introduced in [21]. The main shortcoming of the proposed Z-source circuit breakers is unidirectional conduction capability, which is a severe restriction in dc microgrids. Three structures for bidirectional Z-source circuit breaker are proposed in [23] and [24]. However, performance of these topologies is not evaluated, in practice, and they can be improved from complexity and cost points of view. Some other defects of the proposed structures for the Z-source circuit breakers are lack of a common ground between the load and power source and drawing large fault transient from the generation source.

In this paper, a novel dc bidirectional fault current limiter and interrupter (FCLI) using Z-source topology is proposed, by which a common ground between the load and source is realized. The proposed FCLI is a multifunction breaker, by which circuit breaking, power flow direction control, fault current limiting, and interrupting can be performed. Principle operation of the FCLI is presented in detail for the different operation modes. Furthermore, the performance of the FCLI is evaluated in different conditions using some simulations and experiments. The main advantages of the proposed FCLI are having simple and reliable structure, fast response time of fault current limitation and interruption, and negligible conduction loss.

II. Z-Source Circuit Breakers: A General Overview

A. Unidirectional Z-Source Breaker

Z-source circuit breakers can be broadly categorized into crossed, parallel, and series topologies. In Fig. 1, the three topologies are presented, which are unidirectional circuit breakers [21]. As shown in this figure, a Z-source circuit breaker consists of an SCR and some *L–C* connections, which provide current path for performing natural commutation. Since different topologies have similar operation principle, here only operation of the series topology is discussed in detail. As shown in Fig. 1(c), when a fault is introduced in output of the Z-source breaker, the Z-source capacitors cannot be short-circuited due to the Z-source inductors. Since the inductor currents cannot change instantaneously, high-frequency current passes through the Z-source capacitors and the SCR as shown in red. If the Z-source capacitors current magnitude reaches the inductor current, the SCR current goes to zero. In this condition, the SCR commutates off naturally and the *L–C* branches form a resonance circuit, which supplies the fault by a descending fault current. When polarity of the inductors changes, the antiparallel diodes turn on and the inductors energy dissipates in the parallel resistors. Therefore, the Z-source breaker can limit and interrupt fault current without any stress on the device.

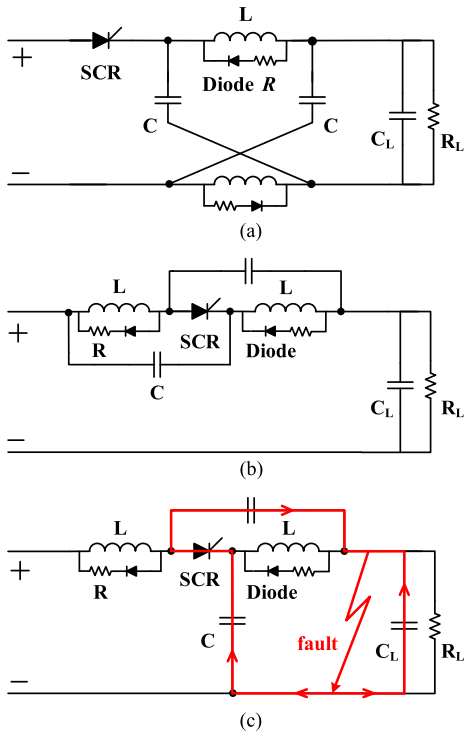

Fig. 1. Unidirectional Z-source circuit breakers: (a) Crossed Z-source, (b) parallel Z-source, and (c) series Z-source circuit breakers proposed in [21].

B. Bidirectional Z-Source Circuit Breaker Mode

The unidirectional Z-source circuit breakers have some limitations especially in applications such as dc microgrids. Although bidirectional topologies for Z-source breaker have considerable merits compared with unidirectional topologies, only few topologies have been proposed in this regard. In Fig. 2, three bidirectional Z-source breaker topologies are shown. The three structures have one or two back-to-back SCRs to pass the load current in both directions. Also, these topologies require one or more inductors in the return path of the dc source, which leads to loss of the common ground. In addition, the back-to-back SCR needs several independent drivers, which makes the breaker more expensive.

III. Proposed Topology and Operation Principle

The proposed FCLI is a bidirectional circuit breaker, by which not only functionalities of a conventional dc circuit breaker are realized, but also it can automatically limit and interrupt fault current in both directions. The proposed Z-source breaker has some power components including inductors and SCRs/diodes, which are configured in a way that the load current can be passed through both directions. Moreover, several auxiliary capacitors are utilized in order to realize SCRs commutation as shown in Fig. 3(a). As mentioned, based on the Z-source breaker principle operation, the inductor currents cannot change instantaneously in fault condition, and high-frequency current passes through the Z-source capacitors and the SCR, as shown in red in Fig. 3(b). Therefore, the SCR commutates off, naturally.

Bidirectional operation capability of the proposed topology has some technical justifications. For instance, in a tie feeder

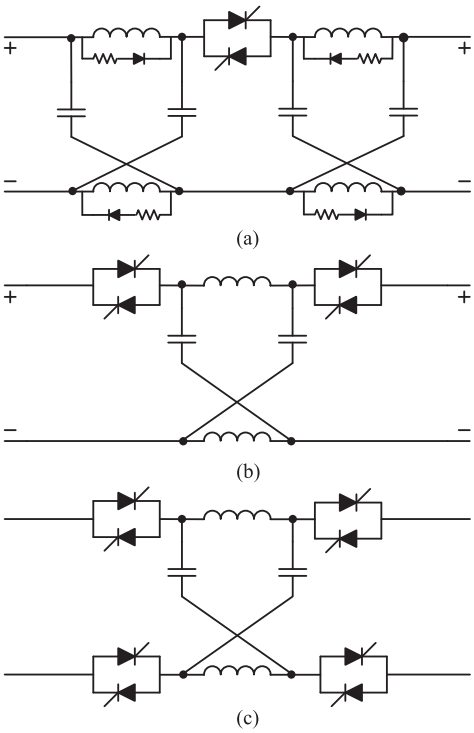

Fig. 2. Three bidirectional Z-source circuit breakers proposed in [23] and [24].

by which two incoming feeders or two adjacent microgrids are connected, utilizing a bidirectional breaker is necessary. Because in this circumstances, not only power flow in both directions is required in normal condition, but also fault current limiting and interruption at the both sides is essential.

Furthermore, the FCLI can interrupt load current by a manual tripping or a control signal through an auxiliary circuit, as shown in blue in Fig. 3(a). Principle of the interruption circuit is similar to the mentioned limitation and interruption mechanism.

A. Fault Current Interruption and Limitation

In normal condition, the breaker connects the load to the power source through the inductors T_1 (or T_2) and D_2 (or D_1), as shown in Fig. 3(a). In this condition, C_0 is charged to the source voltage and voltages of the other capacitors are zero. During initial moments after fault occurrence, the Z-source inductors keep the load current constant. So, fault impedance is supplied by both the load and Z-source capacitors, as shown in Fig. 3(b). The high-frequency current passes through two routes: 1) power supply $C_1 - D_2 - T_1 - C_2 - G_f$ and 2) $C_0 - T_1 - C_2 - G_f$. The total transient currents of C_0 and C_1 are in reverse direction of the SCR current, as shown in Fig. 3(b). This high-frequency current increases until reaches the SCR current. Then, the SCR current goes to zero and commutates off. After the SCR turns off, *L–C* branches create a resonance circuit, as shown in Fig. 3(c).

It should be noted that by decreasing voltage of the inductor (L_1), voltage of D_1 becomes negative and turns off. At this moment, D_2 starts conducting and C_0, L_2, and G_f create a resonance loop. When voltage of C_0 becomes negative, D_2 turns off and negative voltage of C_0 is preserved. In Fig. 3(c),

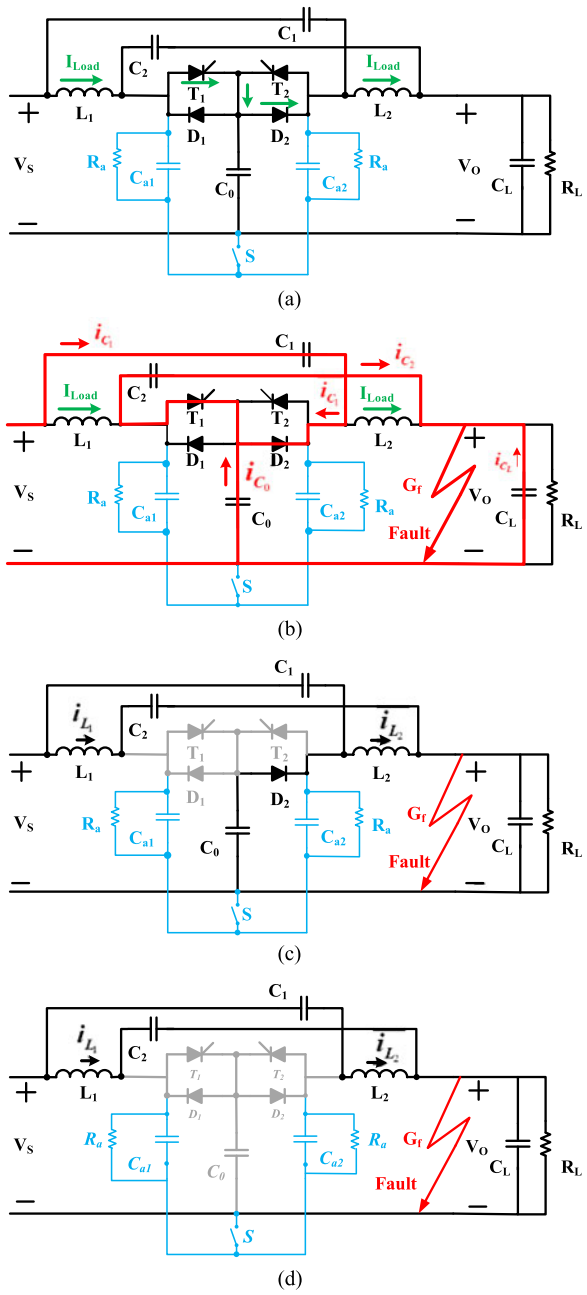

Fig. 3. (a) FCLI in normal condition; different stages in fault current limitation and interruption. (b) First stage. (c) Second stage. (d) Third stage.

there are three resonance paths. After turning off the thyristors and their antiparallel diodes, the resonance circuit relevant to C_0 is removed, as shown in Fig. 3(d). In the last time interval of the fault current limiting and interrupting, the remained energy in the other resonance paths dissipates in the relevant circuits, as shown in Fig. 3(d).

To indicate operation of the proposed dc breaker in more detail, it is assumed that the FCLI protects an *RC* load ($R_L = 20\,\Omega$ and $C_L = 500\,\mu$F) supplied by a low-voltage dc feeder ($V_s = 400$ V). Different voltage and current waveforms of the FCLI are presented in Figs. 4 and 5. As shown in Fig. 4, current of T_1, L_1, D_2, and L_2 are equal to the load current (20 A) in

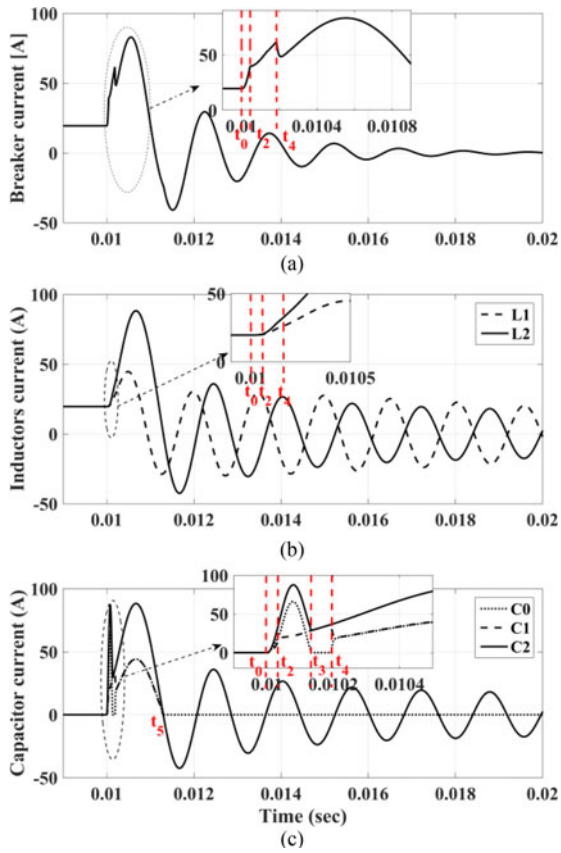

Fig. 4. Different waveforms of the systems in case of a typical fault occurrence: (a) Breaker current, (b) inductors current, and (c) capacitors current.

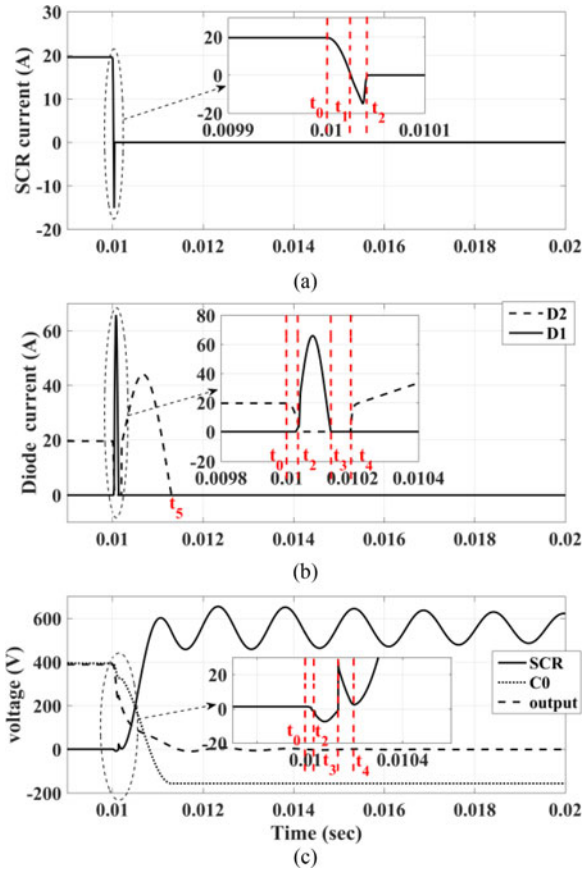

Fig. 5. Some other waveforms of the systems in the fault condition: (a) SCR current, (b) diodes current, and (c) components voltage.

normal condition. A typical fault is introduced in the system with $G_f = 2\,\Omega^{-1}$ and ramp rate $2 \times 10^5\,\Omega^{-1} \cdot \mathrm{s}^{-1}$ at $t = 0.01$ s. The limited fault current of the feeder is shown in Fig. 4(a). As mentioned, currents of the inductors remain constant and currents of the capacitors increase at the initial moments after the fault occurrence during $t_0 - t_2$, as shown in Fig. 4(b) and (c).

At $t = t_1$, current of C_2 becomes equal to current of L_1 and the thyristor is turned off at $t = t_2$, as shown in Fig. 5(a). From Fig. 5(b), it can be observed that after turning off the thyristor, D_2 is turned OFF and D_1 is turned ON. Different voltages of the system are shown in Fig. 5(c). As shown in this figure, at $t_0 - t_3$, voltage of the thyristor is negative which guarantees permanent turning off the thyristor. As mentioned, voltage of C_0 remains negative after turning off D_2. At $t = t_5$, the resonance circuits of C_1 and C_2 resonate and energy of the inductors dissipates in the fault impedance.

At $t = t_1$, current of C_2 becomes equal to current of L_1 and the thyristor is turned off at $t = t_2$, as shown in Fig. 5(a). From Fig. 5(b), it can be observed that after turning off the thyristor, D_2 is turned OFF and D_1 is turned ON. Different voltages of the system are shown in Fig. 5(c). As shown in this figure, at $t_0 - t_3$, voltage of the thyristor is negative which guarantees permanent turning off the thyristor. As mentioned, voltage of C_0 remains negative after turning off D_2. At $t = t_5$, the resonance circuits of C_1 and C_2 resonate and energy of the inductors dissipates in the fault impedance.

B. Load Current Breaking and Manual Tripping

Another important capability of the proposed FCLI is soft tripping of the load current. The FCLI can trip load current by an auxiliary circuit shown in blue in Fig. 3(a). In Fig. 6(a), the involved components in the breaking process are depicted. When the switch is turned on, C_0 is discharged through T_1 and D_2 or T_2 and D_1. Therefore, the thyristors can be commutated off and the feeder current is interrupted by the FCLI. After the SCR turns off, C_0 discharges through D_1 and D_2, as shown in Fig. 6(b). The system waveforms for a typical normal load tripping are presented in Fig. 6(b). It can be observed that the load current is interrupted in a soft tripping during about 10 ms.

C. Comparison Between the Bidirectional Z-Source Circuit Breaker Topologies

Some key features for the Z-source breakers are considered and the bidirectional Z-source circuit breaker topologies are compared in Table I.

The first version of the Z-source circuit breaker provides absolute electric isolation through turning off the SCR. Other series and parallel structures of the Z-source breaker do not provide absolute electric isolation. The main motivation for development of the crossed Z-source breaker is providing common ground between the load and dc source. In spite of the mentioned advantages of the proposed Z-source breaker, it does not have

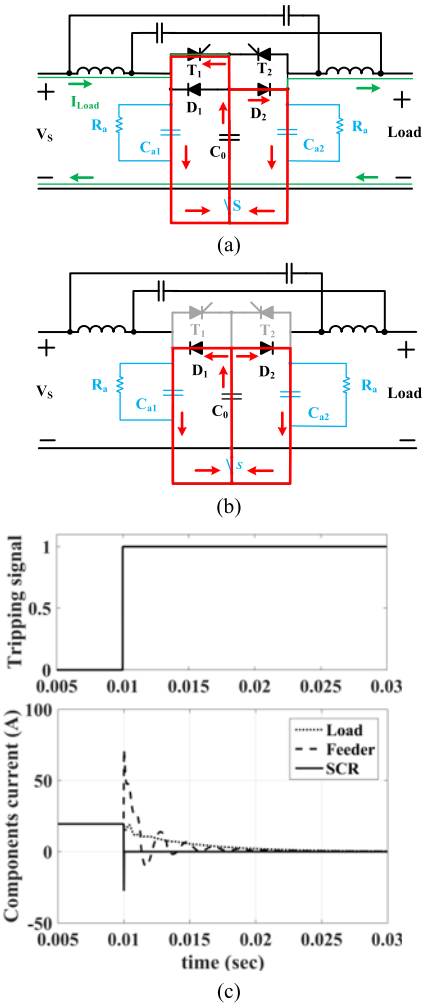

Fig. 6. Different stages in manual tripping: (a) first stage, (b) second stage, and (c) different waveforms of a typical load current interruption.

absolute electric isolation which can be topic of future investigations in this regard. From the comparison, it can be concluded that the proposed topology has a relative superiority over the other structures.

IV. Analysis and Design Framework

In this section, the proposed FCLI operation is analyzed and its design framework is presented in detail. The FCLI is turned on using a pulse command with duration about a few milliseconds. After turning on the breaker and passing the transient state, the breaker conducts the load current with a small voltage drop across the inductors, SCRs (T_1 or T_2), and diodes (D_2 or D_1). Referring Fig. 3(a), in normal condition, we have

$$I_{\text{Load}} = \frac{V_s - v_{f,\text{SCR}} - v_{f,\text{Diode}}}{R_{\text{Load}} + R_{\text{on,SCR}} + R_{\text{on,Diode}} + R_{\text{inductors}}} \tag{1}$$

where V_s, $V_{f,\text{SCR}}$, $V_{f,\text{Diode}}$, R_{load}, $R_{\text{on,SCR}}$, $R_{\text{on,Diode}}$, and $R_{\text{inductors}}$ are source voltage, forward voltage of the SCR, forward voltage of the diode, the load resistance, on-state resistance of the SCR, the diode on-state resistance, and the inductors resistance, respectively.

Detectable magnitude and ramp rate of fault current are the main considerations for the FCLI design, which determines minimum sufficient current to commutate off the SCR. Since fault current rises abruptly and the inductor currents cannot change instantaneously, the Z-source capacitors have the main contribution in the fault current. Minimum required fault current provided by the capacitors for turning off the thyristors is dependent on rising time and amplitude of the fault current. Therefore, the *L–C* components should be designed such that they can handle turning off the thyristors in different fault condition. In the next section, required relations for calculation of these components are derived in a mathematical analysis.

A. Minimum Detectable Fault Conductance

Applying voltage and current Kirchhoff's laws in the aforementioned transient paths, it can be written

$$\frac{dv_o}{dt} = -\frac{C_0 + C_1 + C_2}{C_0 + C_1}\frac{dv_{C_2}}{dt}. \tag{2}$$

For simplicity of the calculation and identical operation of the FCLI in both directions, it is supposed that the Z-source capacitors are equal ($C_0 = C_1 = C_2 = C$). Fault current can be represented in terms of the load current and Z-source capacitors as follows:

$$i_{\text{fault}} = \frac{2C + 3C_L}{3C_L} i_{C_L} \tag{3}$$

$$i_{\text{fault}} = \frac{2C + 3C_L}{2C} i_{C_2}. \tag{4}$$

In order to interrupt the feeder current, i_{C_2} must reach I_{Load}. During initial moments of fault occurrence, i_{Fault} is

$$i_{\text{fault}} = G.V_s. \tag{5}$$

Therefore, assuming zero voltage drop across the breaker and combining (4) and (5) and substituting them into (1) gives

$$G_{\min} = \frac{2C + 3C_L}{2C}.\frac{1}{R_L} \tag{6}$$

where $G_{\min}$ is the minimum detectable fault conductance.

B. Minimum Required Fault Conductance Ramp Rate

It is supposed that the fault conductance increment is linear with slope *k* from zero to *G* during fault time interval. Fault time interval is $t_0 < t < t_0 + \Delta t$, so

$$k = \frac{G}{\Delta t} \tag{7}$$

therefore fault can be presented during fault time interval $t_0 < t < t_0 + \Delta t$ ($t_0 = 0$) as

$$G_f = k.t \tag{8}$$

on the other hand, fault current can be expressed as

$$i_{\text{fault}} = G_f.v_o = k.t.v_o. \tag{9}$$

Substituting (9) into (3), we have

$$k.t.v_o = -\frac{2C + 3C_L}{3C_L}\frac{dv_o}{dt}. \tag{10}$$

TABLE I
COMPARISON OF THE BIDIRECTIONAL Z-SOURCE CIRCUIT BREAKERS

Type	Number of switches	Inductor existence in the return path	Simplicity of the driver circuitry	Overall cost	Having common ground	Reflection of fault current to the source	Coupling isolation from dc power
First structure in [23]	Low	Yes	Low	low	No	High	Turned-off SCR
Second structure in [23]	Medium	Yes	Medium	medium	No	low	Turned-off SCR
Structure in [24]	High	Yes	High	high	No	low	Turned-off SCR
The proposed structure	**Medium**	**No**	**Low**	**Low**	**YES**	**High**	**Series *L–C* coupling**

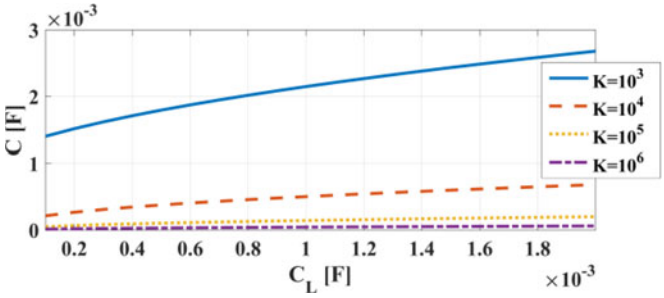

Fig. 7. Minimum required Z-source capacitance for commutation.

Solving (10) yields

$$v_o = V_S e^{-\frac{3}{2}\frac{kt^2}{2C+3C_L}}. \tag{11}$$

Equation (11) is an exponential equation, and it can be simplified by considering two first terms of Taylor's series:

$$v_0 = V_S\left(1 - \frac{3}{2}\frac{kt^2}{2C+3C_L}\right). \tag{12}$$

Also, i_{C_2} can be rewritten as

$$i_{C_2} = \frac{2CV_sk}{2C+3C_L}\left(t - \frac{3}{2}\frac{k}{2C+3C_L}t^3\right). \tag{13}$$

By derivation of (13) and equating it with zero, we have

$$t_{\max} = \sqrt{\frac{2C+3C_L}{4.5k}} \tag{14}$$

where $t_{\max}$ is the instant at which current of C_2 reaches its maximum value. Substituting $t_{\max}$ in (13), maximum current of C_2 is obtained as follows:

$$i_{C_2,\max} = \frac{4V_sC}{3}\sqrt{\frac{k}{4.5\,(2C+3C_L)}}. \tag{15}$$

For having a perfect commutation, current of C_2 should be equal or greater than the inductor current ($i_{C_2,\max} \geq I_{\text{load}}$). Therefore, to calculate minimum detectable fault ramp rate ($k_{\min}$), i_{C_2} should be equal to the load current, so

$$k_{\min} = \frac{81}{32C^2{R_L}^2}\,(2C+3C_L). \tag{16}$$

In Fig. 7, minimum required Z-source capacitance for a perfect commutation versus load capacitance for three fault ramp rates is drawn. It can be observed that for lower fault ramp rates and the loads with higher capacitance, higher Z-source capacitance is needed.

Using (15) or (16), one can calculate the Z-source capacitors to guarantee a perfect commutation for the SCRs. Meanwhile, the time interval at which i_{C_2} more than the inductor current should be greater than reverse-recovery time of the SCRs (t_q).

To calculate Z-source inductors, current of the inductors should be determined as follows:

$$i_L = I_{\text{load}} + \frac{kV_s}{4L\,(2C+3C_L)}t^3. \tag{17}$$

Combining and (13) and (17) yields to

$$i_{\text{SCR}} = I_{\text{load}} - \frac{2CV_sk}{2C+3C_L}t + \frac{kV_s}{2C+3C_L}\left(\frac{1}{4L} + \frac{3Ck}{2C+3C_L}\right)t^3. \tag{18}$$

Therefore, value of the inductors should be large enough that their currents are preserved constant during fault condition. Consequently, the thyristor current should not be affected by the inductor value, so

$$L >> \frac{1}{12k}\frac{2C+3C_L}{C}. \tag{19}$$

Substituting $k_{\min}$ in (19), value of the inductors can be determined as follows:

$$L >> \frac{1}{30}C{R_L}^2. \tag{20}$$

C. Calculation of the Manual Tripping Circuit Components

The resistors R_a are considered several kilohm, by which capacitors C_a are discharged when the switch is open. Value of C_a should be large enough to guarantee a perfect commutation of the thyristors. At initial moments after manual tripping, we have

$$v_{C_0} - \frac{Ri}{2} - v_{C_a} = 0 \tag{21}$$

where R is the resistance of the SCR and diode (which are supposed that become equal). Solving (21), gives

$$i_{C_0} = \frac{2V_s}{R}e^{-\frac{2}{R}\frac{C_a+C_0}{C_aC_0}t}. \tag{22}$$

It is obvious that for commutation of the SCR, i_{C_0} should be raised to $2I_{\text{Load}}$ in less than t_q.

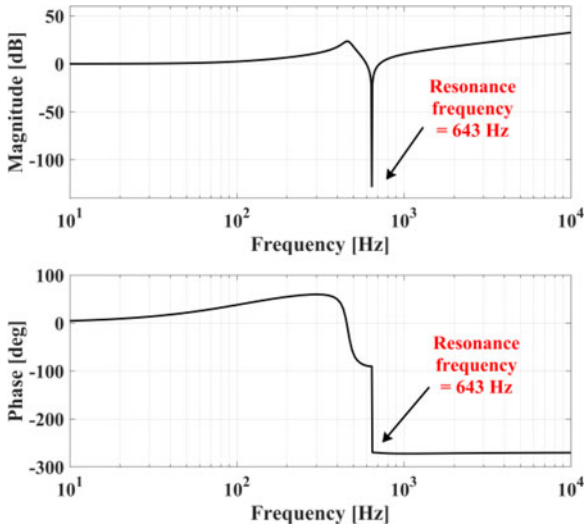

Fig. 8. Bode diagram of the proposed FCLI.

D. Voltage Transfer Function

Since the Z-source breaker may be utilized in the input of a dc motor drive or an inverter, its filter effecting should be analyzed. The output–input voltage transfer function of the proposed FCLI is derived for a resistive load (R). It should be mentioned that the derived transfer function can be developed for any other load types by substituting R with an impedance (Z). From Fig. 3(a), in case of a resistive load, transfer function of the FCLI can be derived straightforwardly as follows:

$$Z_{\text{eq}} = \frac{2RL^2C^2s^4 + 3L^2Cs^3 + 3RLCs^2 + 2Ls + R}{RL^2C^3s^5 + 2L^2C^2s^4 + 2RLC^2s^3 + 3LCs^2 + RCs + 1} \tag{23}$$

$$\frac{v_o}{v_i} = \frac{R}{Z_{\text{eq}}} = R\frac{RL^2C^3s^5 + 2L^2C^2s^4 + 2RLC^2s^3 + 3LCs^2 + RCs + 1}{2RL^2C^2s^4 + 3L^2Cs^3 + 3RLCs^2 + 2Ls + R}. \tag{24}$$

From (24), the FCLI has unity gain with zero phase shift in low frequencies. This behavior can also be concluded from Fig. 3(a), because the inductors and capacitors have low and high impedances in low frequency, respectively. In Fig. 8, amplitude and phase shift of the transfer function are illustrated. In this figure, values of the inductors, capacitors, and load are 900 μH, 68 μF, and 20 Ω, respectively. At the resonant frequency (about 643 Hz in this case), the resonance gain is approximately zero due to the parallel capacitor.

The proposed Z-source circuit breaker has no malfunction in step load change lower than twice of the steady-state current. Although most of the already proposed Z-source breakers suffer from maloperation in step load change higher than twice of the steady-state current, a modification should be accomplished in the proposed Z-source breaker to rectify this shortcoming.

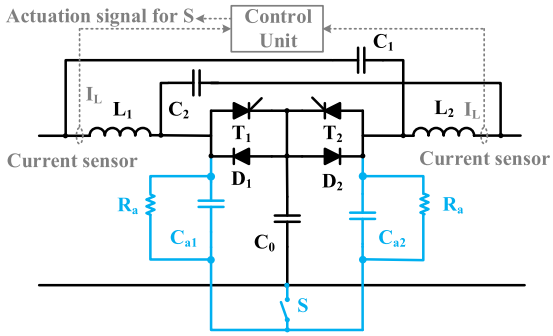

Fig. 9. Proposed bidirectional Z-source breaker with control unit.

Considering minimum detectable fault conductance (calculated by (6)) and minimum required fault conductance ramp rate (calculated by (16)), the Z-source breaker's components are such designed that the breaker does not have maloperation in case of reasonable step load changes. However, for operation of the breaker in case of faults that do not trip the breaker automatically, a control unit is considered. In the control unit, the Z-source inductor current is sensed and compared with prespecified threshold. The manual tripping switch is triggered by the output signal of the comparator in case of faults that do not trip the breaker automatically. The developed structure is shown in Fig. 9.

V. Experimental Results

In order to evaluate the performance of the FCLI, a prototype with lower power scale relative to the simulated one is fabricated. The FCLI is tested in a simple system including a dc voltage source, a feeder, and a load as same as the simulation. The utilized test bench is shown in Fig. 11. The load current and voltage of the power system are 10 A and 20 V, respectively, in normal condition. In the prototype, the load resistance and capacitance are 2 Ω and 500 μF, respectively. Minimum detectable fault ramp rate is supposed $2 \times 10^4\ \Omega^{-1} \cdot \text{s}^{-1}$. Therefore, using (16), the Z-source capacitances are derived 210 μF, which is selected 200 μF in practice. From (20), for the prototype Z-source circuit breaker L should be greater than 26 μH. Choosing an inductance about ten times or more this value is acceptable. In the prototype, Z-source inductance is chosen 500 μH. So, it can limit ramp rate of fault current at incipient moments after fault occurrence, dramatically. Solving (18) for $i_{\text{SCR}} = 0$ gives $t_1 = 0.024 \times 10^{-3}$ s and $t_2 = 0.217 \times 10^{-3}$ s, as shown in Fig. 10. Therefore, an SCR with t_{off} between t_1 and t_2 should be selected. The utilized SCR in the prototype has $t_{\text{off}} = 50\ \mu$s, which fulfill the requirement. For calculation of the auxiliary capacitance of the manual tripping circuit, (22) is utilized. For realizing manual tripping, i_{C_0} should be two times of normal load current which yields $C_a = 177\ \mu$F. In the prototype, C_a is set to 200 μF. For calculation of C_a, it is considered that $t \geq t_{\text{off}}$ and $R = 0.2\ \Omega$. Different parameters of the prototype FCLI and the system specifications are tabulated in Table II.

In the following, three cases are investigated including: 1) the system with and without the FCLI in fault condition in case of a Resistive–Capacitive (RC) load, 2) the system with and without

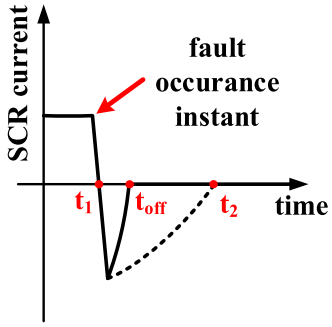

Fig. 10. SCR current in fault condition.

TABLE II
TEST BENCH PARAMETERS

Component	Specifications
SCRs	$I_{T\ (AV)} = 100$ A $t_q = 50\,\mu$s $V_{DMR} = 400$ V
C	200 μF
L	500 μH 20 A
R_a	1.5 kΩ
C_a	200 μF
R_L	2 Ω
C_L	500 μF
R_L	2 Ω
L_L	500 mH

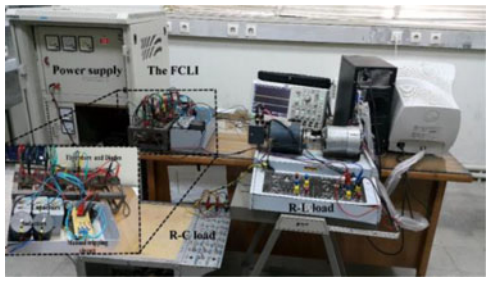

Fig. 11. FCLI in the utilized test bench.

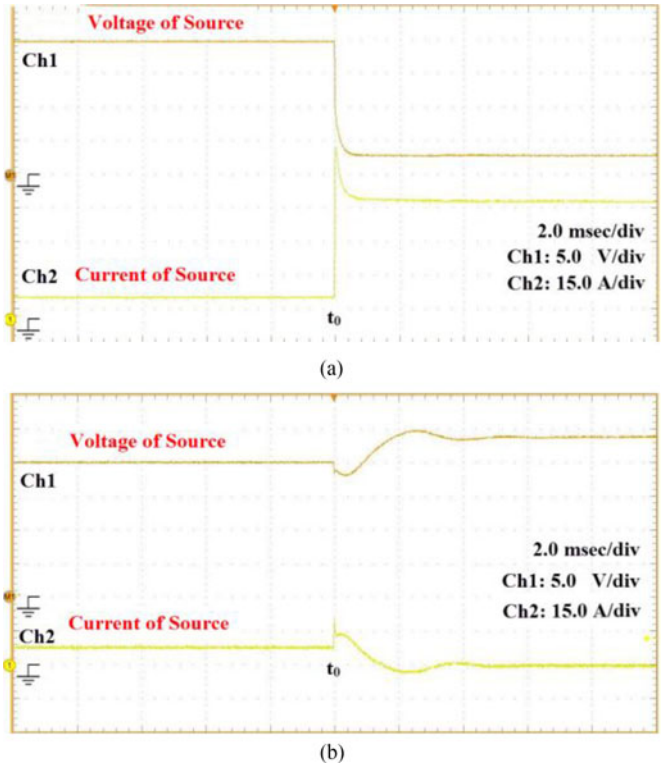

Fig. 12. Voltage and current of the feeder, with and without the FCLI in fault condition with an *RC* load: (a) Without the FCLI and (b) with the FCLI.

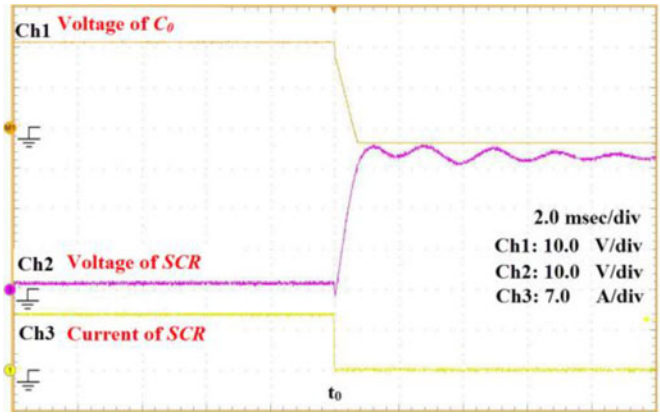

Fig. 13. Voltage and current of the SCR (T_1) as well as voltage of C_0 in case 1 with the FCLI.

the FCLI in fault condition in case of a Resistive–Inductive (*RL*) load, and 3) interruption of the normal load current with the FCLI in case of the *RC* and *RL* loads. In Fig. 12, voltage and current of the source relevant to case one are presented. As shown in Fig. 12(a), the load current and voltage are 10 A and 20 V, respectively, in normal condition. At t_0, a solid fault is applied to the load terminal. Without the FCLI, the feeder current has an overshoot about 70 A due to the load capacitance, which lasts in order of microseconds. Moreover, the steady-state fault current is 50 A, which is about five times of the load current in normal condition. It should be mentioned that the fault current is limited by the inherent resistance of the system. That is why voltage of the feeder is not zero in fault condition. In Fig. 12(b), the same experiment with the FCLI is performed. As shown in this figure, fault current is limited and interrupted in less than 4 ms. The negligible overshoot of the fault current in this case is relevant to the Z-source capacitance. Variation of voltage and current of the feeder during fault occurrence until full interruption is related to step response of the *RLC* circuit formed by the Z-source components. Fig. 13 presents voltage and current of the SCR as well as voltage of C_0 in case of fault current limitation and interruption, as shown in Fig. 12(b). As shown in this figure, current and voltage of the SCR go to about zero and 30 V, respectively. Voltage of C_0 settles in negative value, which causes voltage of the SCR to be greater than the source voltage. The oscillation of the SCR voltage after the interruption is related to step response of the *RLC* circuit, which is damped after several milliseconds. In Fig. 14, voltage and current waveforms of the load are depicted. As shown in this figure, voltage and current of the load reach zero after a transient depending on the fault resistance as well as load and

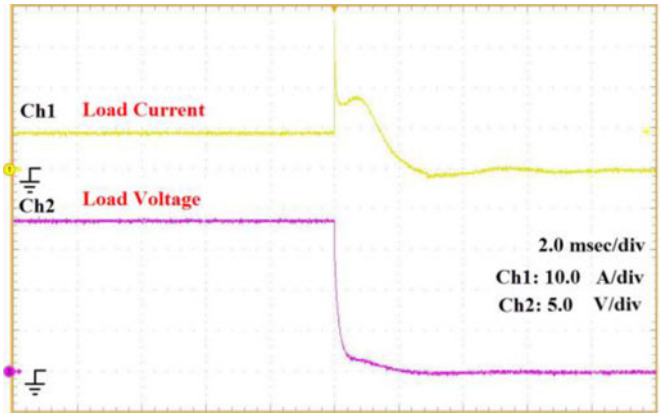

Fig. 14. Load voltage and current waveforms.

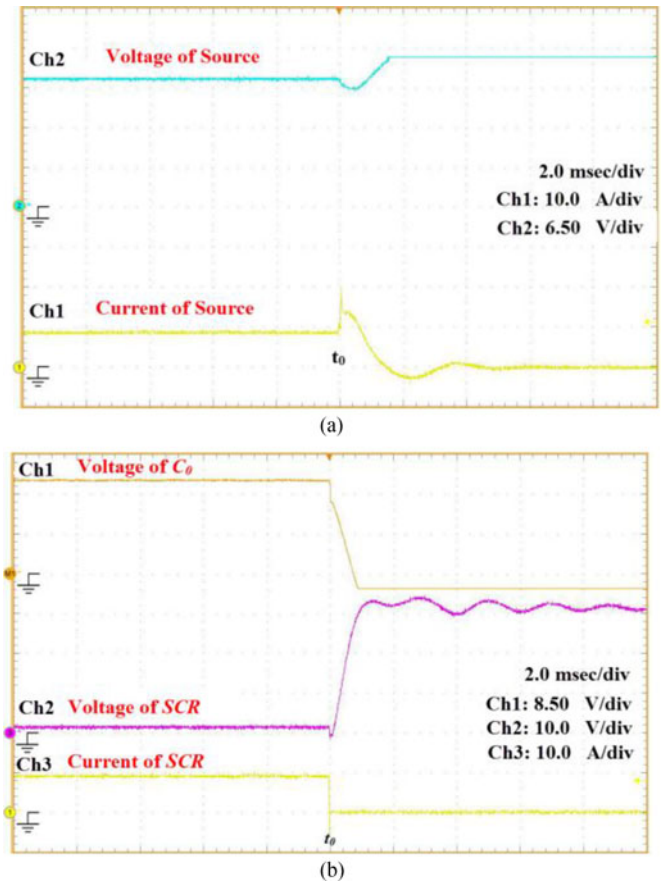

Fig. 15. Operation of the FCLI in case 2: (a) Voltage and current of the feeder and (b) voltage and current of the SCR (T_1) as well as voltage of C_0.

Z-source circuit characteristics. The proposed Z-source breaker can limit and interrupt fault current in case of fault occurrence in both sides of the device. Considering the symmetric structure of the proposed Z-source breaker, this capability is expected obviously. The same results for the FCLI in case 2 are shown in Fig. 15, one can observe that the FCLI is able to limit and interrupt fault current in case of motor load properly.

In Fig. 16, the performance of the FCLI in case of manual tripping is presented. The trip signal is issued at t_0 and it is

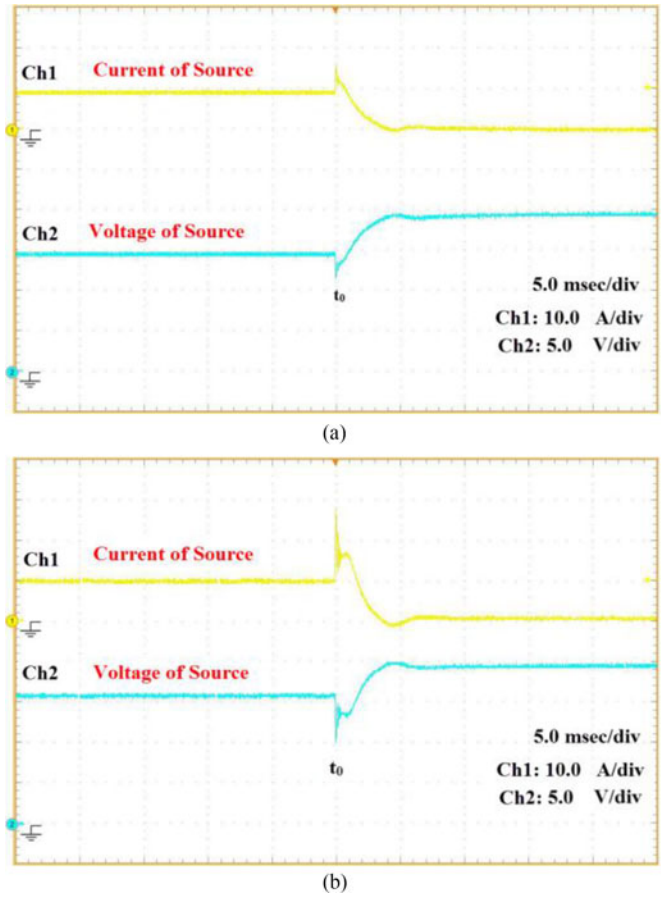

Fig. 16. Manual tripping by the FCLI in case 3: (a) With an *RC* load and (b) with an *RL* load.

observed that the FCLI interrupts load current in a soft interruption. By comparison of the experimental results with the simulation ones, one can conclude that a good accordance is between the results.

From the presented simulation and experimental results, one can observe that the resonant current across the *L* and *C* components does not have considerable impact on the dc source and load waveforms.

VI. Conclusion

In this paper, a novel bidirectional Z-source dc circuit breaker was presented. The proposed Z-source breaker provides common ground for load and power supply. Due to simple structure of the proposed FCLI, it is reliable and cost efficient. The FCLI can handle four main functions including fault current limiting and interrupting, power flow direction control, and circuit breaking. Using the presented analytical analysis for the FCLI, the required relations for calculation of the components and interpretation of the FCLI behaviors in different conditions are derived. The performance of the FCLI is evaluated using some simulations and experiments in different conditions. The results confirm that the FCLI can limit and interrupt fault current without imposing any considerable stress on the system. Moreover, it can interrupt normal load current in a soft-breaking process.

REFERENCES

[1] M. S. Mahmoud, M. S. U. Rahman, and F. M. A. L. Sunni, "Review of microgrid architectures—A system of systems perspective," *IET Renewable Power Gener.*, vol. 9, no. 8, pp. 1064–1078, Nov. 2015.

[2] B. S. Hartono, Y. Budiyanto, and R. Setiabudy, "Review of microgrid technology," in *Proc. 2013 Int. Conf. Qual. Res.*, Yogyakarta, Indonesia, 2013, pp. 127–132.

[3] S. S. Thale, R. G. Wandhare, and V. Agarwal, "A novel reconfigurable microgrid architecture with renewable energy sources and storage," *IEEE Trans. Ind. Appl.*, vol. 51, no. 2, pp. 1805–1816, Mar./Apr. 2015.

[4] L. Che, M. Shahidehpour, A. Alabdulwahab, and Y. Al-Turki, "Hierarchical coordination of a community microgrid with AC and DC microgrids," *IEEE Trans. Smart Grid*, vol. 6, no. 6, pp. 3042–3051, Nov. 2015.

[5] E. Planas, J. Andreu, J. I. Gárate, I. M. De Alegría, and E. Ibarra, "AC and DC technology in microgrids: A review, " *Renewable Sustainable Energy Rev.*, vol. 31, no. 43, pp. 726–749, Mar. 2015.

[6] J. J. Justo, F. Mwasilu, J. Lee, and J. W. Jung, "AC-microgrids versus DC-microgrids with distributed energy resources: A review, " *Renewable Sustainable Energy Rev.*, vol. 31, no. 24, pp. 387–405, Aug. 2013.

[7] T. Dragičević, X. Lu, J. C. Vasquez, and J. M. Guerrero, "DC microgrids—Part II: A review of power architectures, applications, and standardization issues," *IEEE Trans. Power Electron.*, vol. 31, no. 5, pp. 3528–3549, May 2016.

[8] M. Monadi, M. A. Zamani, J. I. Candela, A. Luna, and P Rodriguez, "Protection of AC and DC distribution systems Embedding distributed energy resources: A comparative review and analysis," *Renewable Sustainable Energy Rev.*, vol. 30, no. 51, pp. 1578–1593, Nov. 2015.

[9] R. M. Cuzner and G. Venkataramanan, "The status of DC micro-grid protection," in *Proc. 2008 IEEE Ind. Appl. Soc. Annu. Meet.*, Edmonton, AL, Canada, 2008, pp. 1–8.

[10] S. Lee and H. K., "A study on low-voltage DC circuit breakers," in *Proc. 2013 IEEE Int. Symp. Ind. Electron.*, Taipei, Taiwan, 2013, pp. 1–6.

[11] Z. Ganhao, "Study on DC circuit breaker," in *Proc. 2014 5th Int. Conf. Intell. Syst. Des. Eng. Appl.*, Hunan, China, 2014, pp. 942–945.

[12] R. Ma *et al.*, "Investigation on arc behavior during arc motion in air DC circuit breaker," *IEEE Trans. Plasma Sci.*, vol. 41, no. 9, pp. 2551–2560, Sep. 2013.

[13] L. Liljestrand, M. Backman, L. Jonsson, E. Dullni, and M. Riva, "Medium voltage DC vacuum circuit breaker," in *Proc. 2015 3rd Int. Conf. Electr. Power Equip.-Switching Technol.*, Busan, South Korea, 2015, pp. 495–500.

[14] A. Shukla and G. D. Demetriades, "A survey on hybrid circuit-breaker topologies," *IEEE Trans. Power Del.*, vol. 30, no. 2, pp. 627–641, Apr. 2015.

[15] Z. J. Shen, Z. Miao, and A. M. Roshandeh, "Solid state circuit breakers for DC micrgrids: Current status and future trends," in *Proc. 2015 IEEE 1st Int. Conf. DC Microgrids*, Atlanta, GA, USA, 2015, pp. 228–233.

[16] C. Meyer and R. W. De Doncker, "Solid-state circuit breaker based on active thyristor topologies," *IEEE Trans. Power Electron.*, vol. 21, no. 2, pp. 450–458, Mar. 2006.

[17] Z. J. Shen, G. Sabui, Z. Miao, and Z. Shuai, "Wide-bandgap solid-state circuit breakers for dc power systems: Device and circuit considerations," *IEEE Trans. Electron Devices*, vol. 62, no. 2, pp. 294–300, Feb. 2015.

[18] R. Schmerda, R. Cuzner, R. Clark, D. Nowak, and S. Bunzel, "Shipboard solid-state protection: Overview and applications," *IEEE Electrification Mag.,* vol. 1, no. 1, pp. 32–39, Sep. 2013.

[19] K. A. Corzine and R. W. Ashton, "A new Z-source DC circuit breaker," *IEEE Trans. Power Electron.*, vol. 27, no. 6, pp. 2796–2804, Jun. 2012.

[20] A. Maqsood, A. Overstreet, and K. A. Corzine, "Modified Z-source DC circuit breaker topologies," *IEEE Trans. Power Electron.*, vol. 31, no. 10, pp. 7394–7403, Oct. 2016.

[21] A. H. Chang, B. R. Sennett, A. T. Avestruz, S. B. Leeb, and J. L. Kirtley, "Analysis and design of DC system protection using Z-Source circuit breaker," *IEEE Trans. Power Electron.*, vol. 31, no. 2, pp. 1036–1049, Feb. 2016.

[22] F. Zheng Peng, "Z-source inverter," *IEEE Trans. Ind. Appl.*, vol. 39, no. 2, pp. 504–510, Mar./Apr. 2003.

[23] A. Maqsood and K. Corzine, "The Z-source breaker for fault protection in ship power systems," in *Proc. 2014 Int. Symp. Power Electron., Electr. Drives, Autom. Motion*, Ischia, Italy, 2014, pp. 307–312.

[24] A. Maqsood and K. A. Corzine, "The Z-source breaker for ship power system protection," in *Proc. 2015 IEEE Electr. Ship Technol. Symp.*, Alexandria, VA, USA, 2015, pp. 293–298.

Davood Keshavarzi received the B.Sc. degree in electrical power engineering from Tafresh University, Arak, Iran, in 2014 and the M.Sc. degree in electrical power engineering from Shiraz University, Shiraz, Iran, in 2016. His research field includes power electronics, power electronics application in protection and power quality.

Teymoor Ghanbari received the B.Sc. degree in electrical power engineering from S. R. University, Tehran, Iran, the M.Sc. degree from Shahrood University of Technology, Shahrood, Iran, and the Ph.D. degree in the same field from Shiraz University, Shiraz, Iran. He is currently an Assistant Professor in the School of Advanced Technologies of Shiraz University. His research interests include distributed generation, power electronics, and electrical machines.

Ebrahim Farjah received the B.Sc. degree in electrical and electronics engineering from Shiraz University, Iran, in 1987, the M.Sc. degree in electrical power engineering from Sharif University of Technology, Tehran, Iran, in 1989, and the Ph.D. degree in electrical engineering from Grenoble Institute of Technology, Grenoble, France. He is currently a Professor in the Department of Electrical and Computer Engineering of Shiraz University. His research interests include power electronics, renewable energy, micro-grids, and power quality.